Mechanistic Understanding of CaO-Based Sorbents for High-Temperature CO_2 Capture: Advanced Characterization and Prospects

Maximilian Krödel[+],[a] Annelies Landuyt[+],[a] Paula M. Abdala,[a] and Christoph R. Müller*[a]

Carbon dioxide capture and storage technologies are short to mid-term solutions to reduce anthropogenic CO_2 emissions. CaO-based sorbents have emerged as a viable class of cost-efficient CO_2 sorbents for high temperature applications. Yet, CaO-based sorbents are prone to deactivation over repeated CO_2 capture and regeneration cycles. Various strategies have been proposed to improve their cyclic stability and rate of CO_2 uptake including the addition of promoters and stabilizers (e.g., alkali metal salts and metal oxides), as well as nano-structuring approaches. However, our fundamental understanding of the underlying mechanisms through which promoters or stabilizers affect the performance of the sorbents is limited. With the recent application of advanced characterization techniques, new insight into the structural and morphological changes that occur during CO_2 uptake and regeneration has been obtained. This review summarizes recent advances that have improved our mechanistic understanding of CaO-based CO_2 sorbents with and without the addition of stabilizers and/or promoters, with a specific emphasis on the application of advanced characterization techniques.

1. Introduction

Anthropogenic emissions of CO_2 have increased substantially since the industrial revolution.[1] As a result, the atmospheric CO_2 concentration has reached 410 ppm in 2019.[1–3] Reaching the goal of the Intergovernmental Panel on Climate Change (IPCC) of limiting global warming to 1.5 °C until 2050 requires a significantly less CO_2 intensive society and industry than the ones we have now.[1,4] Besides the transition to renewable energy sources, the application of carbon dioxide capture and storage (CCS) is key to mitigate CO_2 emissions. The IPCC estimates that CCS can contribute up to 20% to the 2050 CO_2 reduction goals.[1] Combined with CO_2 utilization technologies, CCS provides also the means for a circular carbon-based economy, e.g. through the production of (close-to) carbon-neutral methanol.[5–8]

Calcium oxide-based solid sorbents that undergo cyclic carbonation and calcination reactions during CO_2 capture and regeneration, viz. $CaO + CO_2 \leftrightarrow CaCO_3$ with $\Delta_R H^0_{298K} = \pm 179\ kJ\,mol^{-1}$, have emerged as a cost-efficient class of CO_2 sorbents.[9–12] On the process level, the use of CaO-based CO_2 sorbents is referred to as calcium looping (CaL). Techno-economic analyses have provided evidence that the CaL process for CO_2 capture is competitive to the established amine-scrubbing process. Mackenzie et al.[13] estimated the capture costs to be as low as 20 USD per tonne of CO_2 and identified the cyclic CO_2 uptake capacity of the sorbents as a key metric determining the capture costs. However, under realistic process and testing conditions, CaO-based sorbents (mostly limestone-derived) show rapid deactivation over repeated carbonation and calcination cycles, with a residual uptake of $0.05\ g_{CO_2}/g_{CaO}$ after 500 calcination-carbonation cycles.[14] The asymptotic value of the CO_2 uptake was found to be independent of the process conditions, although the rate of the decay in the CO_2 uptake does depend strongly on the calcination and carbonation conditions.[14]

Initial research efforts on CaL focused on natural limestone as the sorbent material. More recently, the development of synthetic CaO-based CO_2 sorbents has gained momentum.[15–20] A number of approaches have been proposed to improve the cyclic stability and residual CO_2 uptake capacity of CaO-based sorbents, including the addition of promoters or stabilizers as well as the micro- and nanostructuring of the sorbents.[16–18,21–26] Several reviews have summarized the engineering strategies to promote or stabilize the CO_2 uptake.[9,12,27] However, our fundamental knowledge of the underlying mechanisms that control the CO_2 uptake characteristics of CaO is limited. Indeed, even the different kinetic regimes in the carbonation reaction and the morphological changes occurring during the carbonation and calcination of bare CaO and $CaCO_3$ are not fully understood.

Recently, the introduction of advanced characterization techniques such as high-resolution transmission electron microscopy (HR-TEM), and HR scanning electron microscopy (SEM),

[a] M. Krödel,[+] A. Landuyt,[+] Dr. P. M. Abdala, Prof. Dr. C. R. Müller
Department of Mechanical and Process Engineering, Laboratory of Energy Science and Engineering
ETH Zürich
Leonhardstrasse 21, 8092 Zürich (Switzerland)
E-mail: muelchri@ethz.ch

[+] The authors contributed equally to this work.

This publication is part of a Special Issue entitled "Green Carbon Science: CO_2 Capture and Conversion". Please visit the issue at http://doi.org/10.1002/cssc.v13.23.

electron-dispersive X-ray spectroscopy (EDX), in-situ X-ray diffraction (XRD), X-ray photoelectron spectroscopy (XPS) and nuclear magnetic resonance (NMR) spectroscopy has shed light on the functioning of CaO-based CO_2 sorbents during CO_2 uptake and regeneration. This review aims at summarizing recent advances in obtaining a fundamental understanding of structural and morphological changes that occur in CaO-based CO_2 sorbents over cyclic operation and in addressing the question to what extent specific structural and morphological features control their CO_2 uptake characteristics. In this respect, an in-depth understanding of the evolution of the sorbents at the Ångstrom to micrometer scale, depicted in Figure 1, is critical to advance the design of next generation CaO-based CO_2 sorbents.

2. Morphological and Structural Evolution of CaO–$CaCO_3$ Sorbents During Operation

The carbonation reaction of CaO occurs in two stages (Figure 2a): I) a fast, kinetically-controlled regime, that is followed by II) a significantly slower, diffusion-controlled regime.[28,29] The transition between the two regimes has been linked to a critical product layer thickness.[29] Most works report a calculated critical product layer thickness in the range of 20–50 nm, although these values are obtained through estimations using simple (bulk) morphological models, in which a product layer is assumed to be a homogenous, continuous and flat layer.[29–31] Furthermore, the total pore volume and surface area of the sorbent rapidly decrease in the kinetically-controlled regime due to the large difference in molar volume between CaO (16.7 cm^3/g) and the product $CaCO_3$ (36.9 cm^3/g). Hence, it has been argued that the initial pore volume critically influences the CO_2 capacity of the sorbent.[26,32,33] For a given "family" of a CaO-based sorbent, a larger initial pore volume (in pores with $d_{pore} < 100$ nm) often results in higher CO_2 uptakes (e.g., for CaO-based sorbents with an inverse opal type morphology,[26] see Figure 2b). Nevertheless, when plotting the initial pore volume ($d_{pore} < 100$ nm) versus the CO_2 uptake in the first cycle for a range of different CaO-based sorbents no obvious correlation between the CO_2 uptake and the initial pore volume of the sorbent can be found (Figure 2b). The same finding can be made when plotting the same data over the BET surface area, determined before the first carbonation step, see Figure 2c. Therefore, recent studies have introduced advanced characterization techniques, including in-situ X-ray techniques and atomic force microscopy (AFM), in an attempt to identify the structural and morphological features that exhibit a direct relationship to the CO_2 uptake and, in general, to obtain a more fundamental understanding of the processes occurring on the atomic scale during the carbonation and calcination reaction.[34–37]

2.1. The relationship between the CO_2 uptake of CaO and its microstructure

Advanced characterization tools have proven to be instrumental to understand the relationship between the microstructure and

Maximilian Krödel obtained his degrees in mechanical engineering (B.Sc.) and process engineering (M. Sc.) from RWTH Aachen with stays at CSIRO (Melbourne, Australia) and the Lawrence Berkeley National Laboratory (Berkeley, USA). Since 2019 he is a PhD student in the department of mechanical and process engineering at ETH Zurich focusing on obtaining structure-property relationships of CaO and MgO-based CO_2 sorbents.

Annelies Landuyt obtained her Bachelor and Master degrees in chemistry from Ghent University. She performed her diploma thesis on the synthesis and characterization of perovskite nanocrystals under the supervision of Prof. Kovalenko at ETH Zürich. In 2019, she joined the laboratory of energy science and engineering as a PhD candidate and is currently focusing on the synthesis and structure-activity studies of MgO and CaO-based CO_2 sorbent.

Paula M. Abdala studied chemical engineering at UTN-Mendoza, Argentina (2002) and obtained her PhD in material science from the UNSAM, Buenos Aires, Argentina (2010), studying structure–performance relationships in materials for solid oxide fuel cells. She then moved to France, where she worked as a postdoctoral researcher at the European Synchrotron Radiation Facility. She joint Christoph Müller's group at ETH Zurich, Switzerland, in 2014 where she is currently employed as a scientist. Her research focuses on obtaining structure–performance relationships in CO_2 sorbents and catalysts for CO_2 valorization using advanced X-ray based characterization techniques.

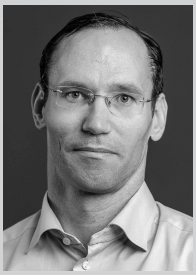

Christoph Müller obtained a diploma in mechanical/process engineering from TU Munich in 2004 and a PhD in chemical engineering from the University of Cambridge in 2008, under the supervision of Prof. John Dennis. In 2010, he became assistant professor at the department of mechanical and process engineering at ETH Zürich. Since 2018, he is full professor at the same institution. His research group is active in the development of CO_2 sorbents and catalysts as well as studying single- and multiphase granular flows.

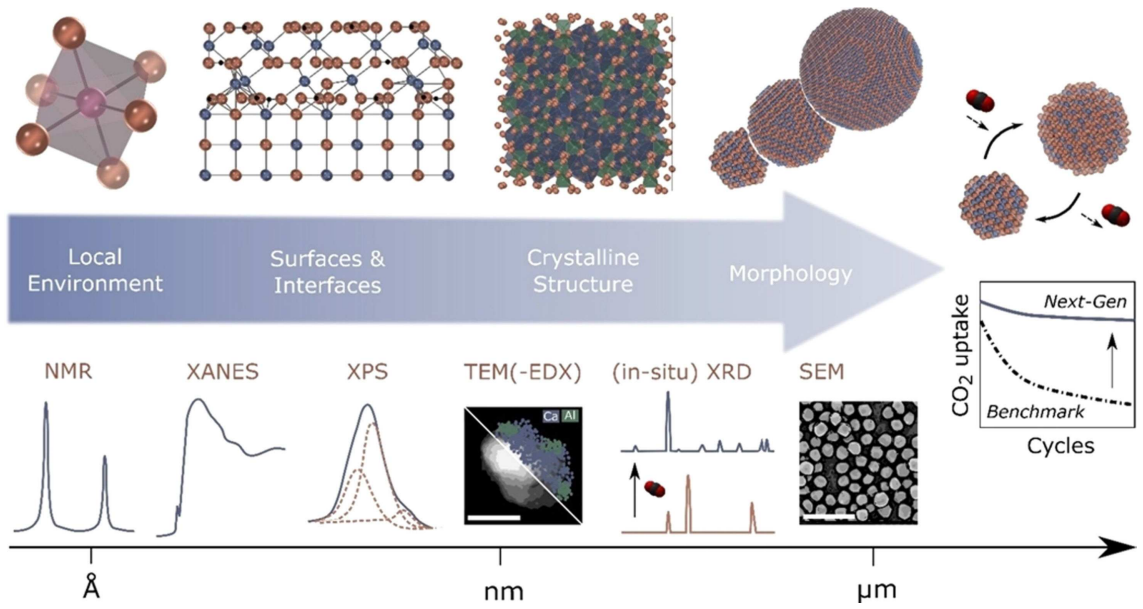

Figure 1. Key characterization techniques to determine the structure of CaO-based sorbents at different length scales providing insight required for the rational design of next generation CaO-based sorbents.

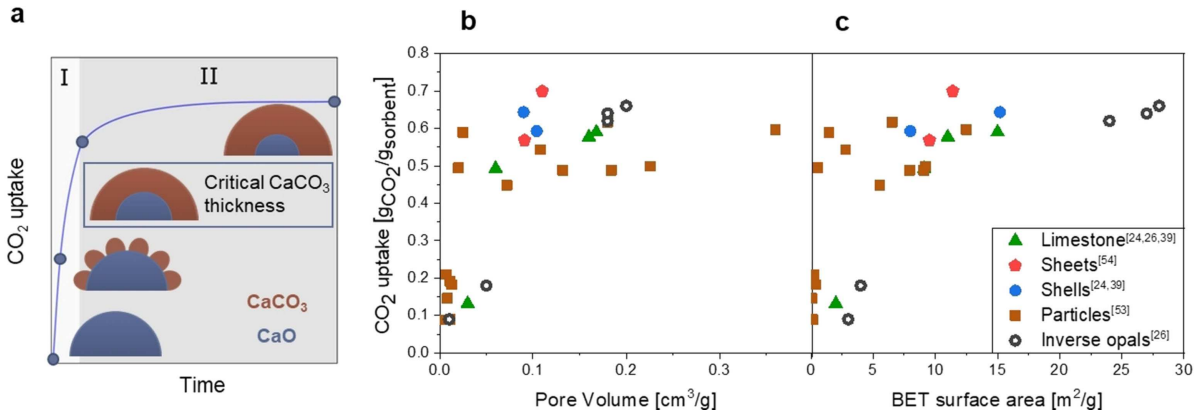

Figure 2. (a) Schematic of $CaCO_3$ product formation during the carbonation of CaO in the kinetically- and diffusion-controlled carbonation regimes and plot of CO_2 uptake as a function of pore volume (b) and surface area (c) for a range of different pure (i.e., only CaO-containing) CaO-based CO_2 sorbent materials.

the CO_2 uptake performance of CaO-based sorbents. For instance, synchrotron-based studies under reaction conditions (in-situ) or after having exposed the materials to reaction conditions (ex-situ) have been carried out to identify relationships between the porosity, crystallite size and the CO_2 uptake performance of CaO-based sorbents.[35–37] For example, Benedetti et al. applied ex-situ synchrotron small angle X-ray scattering (SAXS), ultra small angle X-ray scattering (USAXS) and wide angle X-ray scattering (WAXS) on CaO-based sorbents to study their microstructural features (Figure 3a).[35] Specifically, SAXS and USAXS probed the sorbents' microstructural properties such as pore size distribution, specific surface area and pore radius of gyration. (U)SAXS can be performed simultaneously with WAXS, from which the crystalline phases of a given material can be identified. The ex-situ investigation of the micro-textural properties in a series of CaO samples with different degrees of carbonation showed that the surface area decreases linearly with increasing CaO conversion, confirming the important role of the CaO surface area on the overall CO_2 capacity of a sorbent. However, the relevance of larger (> 100 nm) pores for the CO_2 uptake performance was not elucidated. Furthermore, studying the morphological and structural changes using in-situ methods (i.e., during the reaction of CaO with CO_2 and during the release of CO_2 from $CaCO_3$) can provide time-resolved insight into the structural evolution of the sorbents.

Dunstan et al.[36] investigated the morphological changes in the macro-porous range during CaO carbonation by in-situ synchrotron X-ray tomography. Owing to the different densities of CaO and $CaCO_3$ a phase contrast is visible. The macro-porous network in CaO particles before and after carbonation is visualized in Figure 3b. This experiment clearly evidenced that

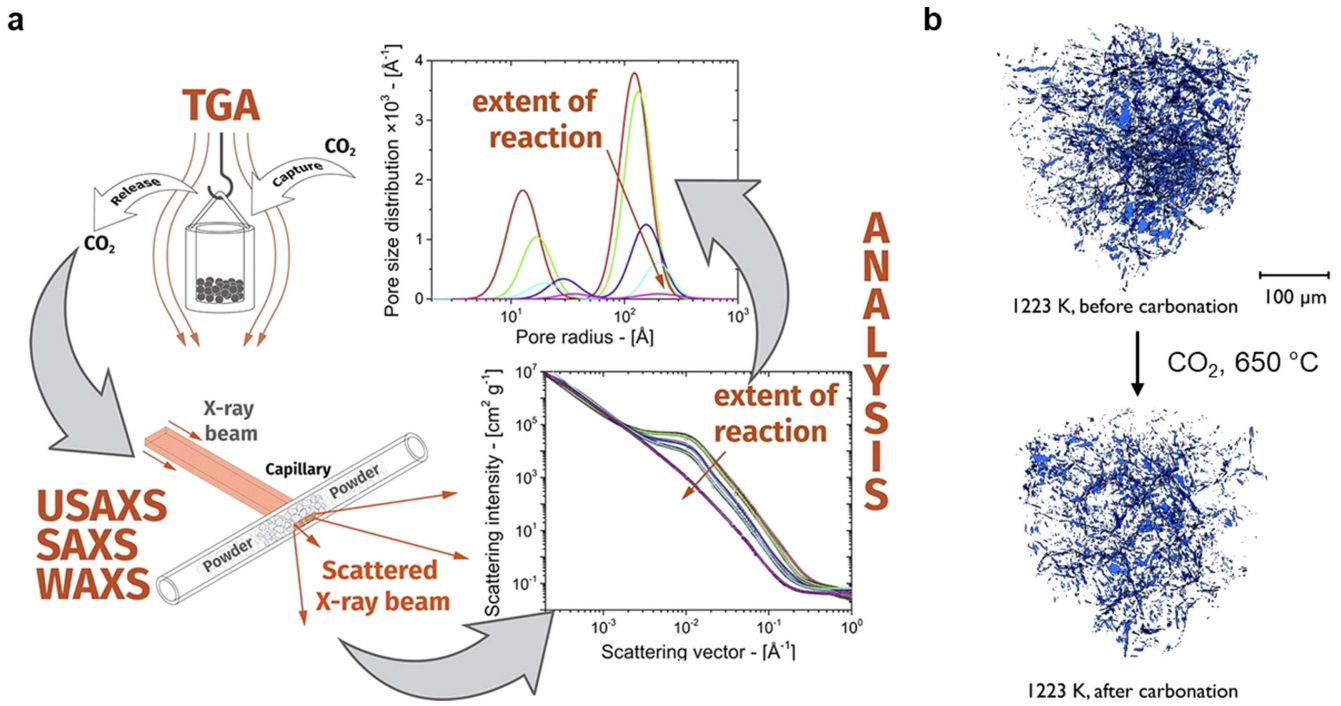

Figure 3. (a) Illustration of the methodology used to quantify changes in pore size distribution during carbonation of CaO by USAXS-SAXS. Reprinted with permission from Ref. [35]; copyright Elsevier, 2019. (b) Visualization of the macro-pores in a CaO particle prior to and after carbonation. Adapted with permission from Ref. [36]; copyright Royal Society of Chemistry, 2016.

also the volume in macro-pores reduces after 50 min of carbonation at 650 °C in 100 % CO_2. It has also been argued that apart from the porosity and the surface area, the CaO/$CaCO_3$ crystallite size can influence the carbonation kinetics.[37,38] The effect of the crystallite size of CaO/$CaCO_3$ on their reactivity was investigated by Biasin et al. utilizing in-situ time resolved (0.25 s acquisition time) synchrotron XRD allowing to determine the rates of $CaCO_3$ formation.[38] Here, the carbonation kinetics of CaO-based sorbents of varying initial crystallite sizes were investigated and the degree of CaO conversion was determined by Rietveld refinement. The authors reported an inverse proportionality between the conversion of CaO in the first cycle and the initial crystallite size of CaO. It was hypothesized that smaller CaO crystallites increase the total length of crystallite boundaries when normalized by the surface area; and that the number of "reactive" sites for the CaO–CO_2 reaction depend not only on the surface area, but also on the length of crystallite boundaries. An interpretation of this observation is that grain boundary diffusion of CO_2 controls to some extent the rate of CaO conversion. However, this hypothesis needs further investigation.

Sintering induced deactivation is a major drawback in CaO-based sorbents; and the underlying sintering process and identification of the key parameters controlling its rate remain under investigation. Sintering can be assessed by following the CaO crystallite size (e.g., under realistic calcination conditions under high partial pressures of CO_2).[14,24,39] For example, Valverde et al.[40,41] studied the calcination of limestone in CO_2 partial pressures (0.05–0.9 bar) and temperature conditions near equilibrium ($P/P_{eq} \lesssim 1$) by in-situ XRD. They found that at low conversions, an intermediate metastable CaO* phase is present, which forms during the desorption of CO_2 and is characterized by a preferred orientation of CaO in the [110] direction.[42] The proposed exothermicity of the CaO* to CaO transformation and the high CO_2 partial pressure were suggested to delay the nucleation of CaO. As the calcination temperature is well below the Tamman temperature (T_T; an indication for the onset of sintering) of CaO ($T_T = 1310$ °C),[12] the authors concluded that the observed CaO crystallite growth during calcination in CO_2 is mainly a consequence of the sintering of the metastable CaO* phase rather than that of the final CaO.

2.2. $CaCO_3$ product layer formation

A crucial aspect of the kinetics of the carbonation reaction is the growth mechanism of the $CaCO_3$ product on the CaO surface. Hypothetically, $CaCO_3$ can grow on CaO as a uniform layer, in the form of islands or in a combination of both modes.[34,43] A study by Li et al.,[34] in which CaO single crystals were carbonated at different temperatures and subsequently analyzed by AFM, tentatively indicates that $CaCO_3$ starts to grow in the form of islands, which eventually merge. As displayed in Figure 4a, the size and distribution of the $CaCO_3$ islands depends on the carbonation temperature. Higher carbonation temperatures result in larger islands and lower island densities. At high conversions, the islands have merged into a $CaCO_3$ layer that fully covers the CaO surface as visualized

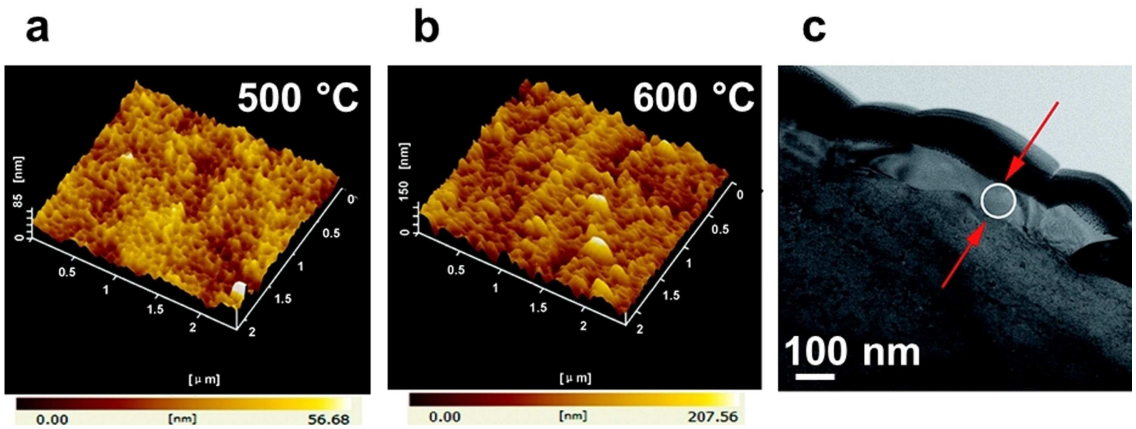

Figure 4. AFM graphs of CaO single crystals after treatment in CO_2 at (a) 500 °C and (b) 600 °C. Adapted with permission from [34]; copyright American Chemical Society, 2012 (c) FIB-TEM image showing the $CaCO_3$ product layer. Adapted with permission from Ref. [44]; copyright Royal Society of Chemistry, 2019.

by FIB-TEM (Figure 4c).[44] Figure 4c shows a CaO particle covered by a $CaCO_3$ layer with a thickness of about 90 nm. A visualization of the morphology of the product layer at the end of the kinetically-controlled reaction regime has not been reported yet, due to the difficulty to 'freeze' the reaction exactly at the transition from the kinetically-controlled to the diffusion-controlled reaction regime.

In the diffusion-controlled regime, a number of diffusion processes, including grain boundary and bulk diffusion govern the rate of the carbonation reaction.[28,45–47] Concerning bulk diffusion, which includes vacancy and interstitial diffusion[43,48] and becomes dominating for longer reaction times, the most likely diffusing species are CO_2, Ca^{2+}, CO_3^{2-} and O^{2-}. Considering that charge balance must be maintained, three diffusion mechanisms can be envisioned, i.e. an inward diffusion of CO_2, a counter diffusion of O^{2-} and CO_3^{2-} or an outward diffusion of both Ca^{2+} and O^{2-} (Figure 5a).[46,48,49] To elucidate the prevailing diffusion mechanism, Sun et al.[49] performed an inert platinum marker experiment by placing a platinum marker on top of a sintered CaO pellet. The pellet was carbonated for 4 months at 650 °C in pure CO_2. SEM-EDX analysis of the reacted pellet shows that the platinum marker is on top of the partially carbonated CaO layer (Figure 5b). From this observation the authors concluded that there is an inward diffusion of CO_3^{2-} and an outward diffusion of O^{2-}. However, the carbonation time of 4 months is unrealistic (a typical carbonation time in a TGA is 20 min, and even shorter in a fluidized bed) for the CaO/$CaCO_3$-system and the implications of this experiment for practical CaL applications are unclear. In addition, the diffusion of CO_2 by a sequential decomposition of neighboring carbonate ions in the product layer was not considered, which could be very effective as the carbonation is performed at temperatures above the T_T of $CaCO_3$ (T_T = 553 °C).

Generally, it is very challenging to distinguish experimentally between the three diffusion mechanisms outlined in Figure 5a. However, ab initio, atomic-scale simulations of diffusion processes in calcite can provide valuable insights. Besson et al.[48] simulated the diffusion of oxygen and the

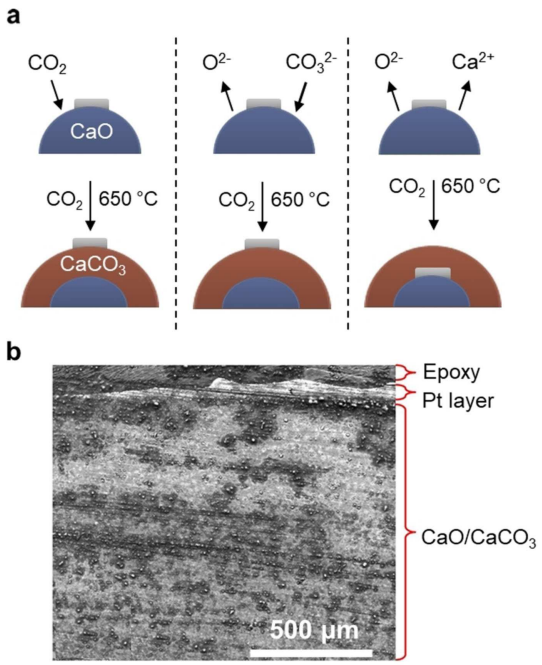

Figure 5. (a) Possible outcomes of an inert marker experiment. (b) SEM image of a cross section of a carbonated CaO pellet after an inert marker experiment. Adapted with permission from Ref. [49]; copyright Elsevier, 2012.

relevant carbon containing species (including CO^-, CO_2 and CO_3^{2-}) in calcite at 527 °C by means of ab-initio calculations. Based on the calculated migration energies for different diffusion pathways of oxygen they found that the transport of oxygen ions in calcite occurs easily (migration energy ~0.5 eV) and is mediated by either an interstitial or an oxygen vacancy mechanism, depending on the thermodynamic conditions. In contrast, the diffusion of carbon containing species requires complex point defects (CPDs; defects in the crystal structure that involve two or more sites). At the investigated temperature (527 °C), the diffusion of CO_2 can be ruled out due to the very

high formation energy of the CO_2 CPD (>2.2 eV). Similarly, the diffusion of CO_3^{2-} via a CPD is associated with a migration energy barrier of 5 eV, which is too high to occur at the given temperature. The authors could not identify an energetically favorable diffusion pathway for carbon containing species in calcite. Note that the outcome of the calculations at the actual carbonation temperature in the CaL process (>600 °C) could be profoundly different. Thus far, no evidence for any of the three diffusion mechanisms sketched in Figure 5a has been reported. Therefore, further theoretical calculations in combination with diffusion experiments on (partially) carbonated CaO model systems under realistic conditions are needed.

3. Recent Advances in the Characterization and Engineering of CaO-Based Sorbents

The engineering of CaO-based sorbents by nanostructuring and the addition of stabilizers or promoters has led to substantial improvements in their CO_2 uptake performance.[9,12] These strategies and our current mechanistic understanding thereof will be discussed in the following sections.

3.1. Nanostructured CaO: towards fast and full conversion

Since CaO-based sorbents derived from naturally occurring precursors such as limestone do not reach full CaO conversion within reasonable timescales and experience rapid deactivation with increasing cycle numbers, intensive efforts are undertaken to design more effective sorbent materials. An ideal CaO-based CO_2 sorbent displays a rapid and (close to) full conversion over many carbonation-calcination cycles.[12,14,50,51] Since a drop in the CO_2 uptake capacity is associated largely with pore blockage due to the large difference in the molar volume between CaO and $CaCO_3$ and diffusion limitations with increasing thicknesses of the carbonate layer, an ideal sorbent should contain a largely meso-porous (≤100 nm particle sizes) morphology.[14,18,21,39,52,53] To this end, template-assisted synthesis approaches have proven to be very useful.[18,24,39,53] For example, Wang et al.[54] used a sacrificial N-doped carbon nanosheet template to synthesize highly macroporous CaO nanosheets (CaN), see Figure 6a. Furthermore, Naeem et al.[24] developed hollow CaO microspheres utilizing spherical, carbonaceous templates (Figure 6b) and Kim et al.[26] obtained inverse opal-type CaO (Figure 6c) relying on carbon nanospheres as templates. These CaO-based materials show an enhanced CO_2 sorption capacity as compared to limestone, with CO_2 uptakes of up to 0.7 $g_{CO_2}/g_{sorbent}$ (Figure 6 d-e). Nevertheless, all three nanostructured materials suffered from sintering-induced deactivation (owing to the lack of a structural stabilizer), which led to a gradual destruction of the structured morphology (and it turn the CO_2 uptake) with cycling. Hence, nanostructuring alone is not sufficient to achieve fast and full conversion over many calcination-carbonation cycles.

3.2. Stabilization and deactivation mechanisms of metal oxide-stabilized CaO-based sorbents

The currently dominating approach to mitigate sintering induced deactivation of CaO is the introduction of high Tammann-temperature metal oxide stabilizers.[9,12,55] It is believed that stabilizers act as physical barriers between otherwise adjacent CaO grains, hence reducing the rate of sintering and stabilizing the pore network and surface area of the sorbent.[23,56,57] Various metal oxides have been explored as stabilizers including Al_2O_3[20,23,26,58–60] (and the respective mixed calcium aluminates $Ca_xAl_yO_z$ that form during calcination[23,25,61]), MgO,[17,18,24,54,62,63] SiO_2,[64–67] TiO_2[68] or ZrO_2.[57,69–72] Stabilizers are commonly added in quantities ranging between 5–20 wt%,

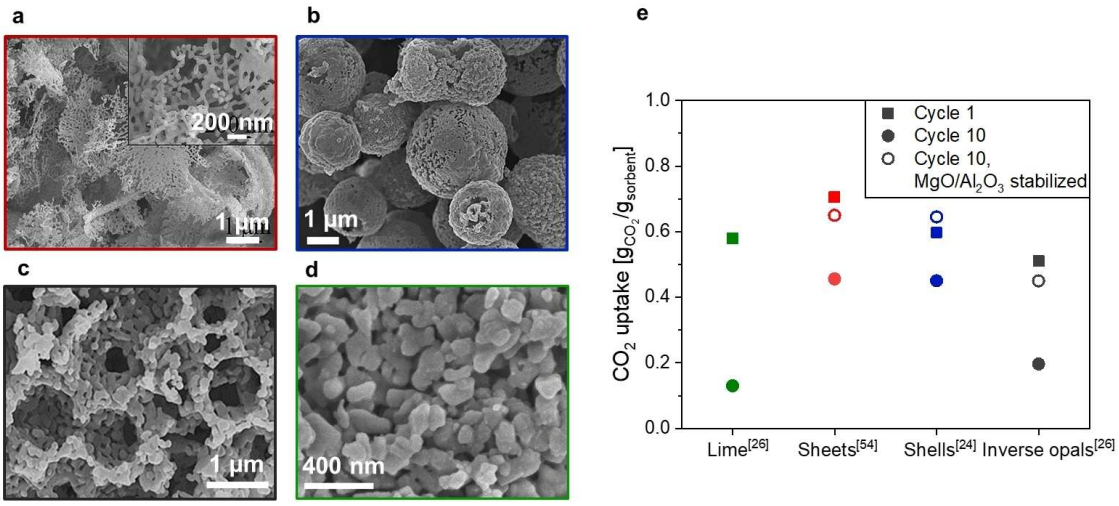

Figure 6. SEM images of (a) CaO nanosheets, (b) CaO microspheres, (c) inverse opal-type CaO and (d) limestone. (e) CO_2 uptake of different CaO materials in the 1st cycle and 10th cycle in presence and absence of a stabilizer. (a) Adapted with permission from Ref. [54]; copyright Elsevier, 2019. (b) and (d) Adapted with permission from Ref. [24]; copyright Springer Nature, 2018. (c) Adapted with permission from Ref. [26]; copyright American Chemical Society, 2019.

with the optimal quantity being a trade-off between the degree of morphological stabilization and the quantity of CO_2 capture-inert material added. The addition of stabilizers has often resulted in significant improvements, in particular during the first few cycles (see Figure 6 e), achieving CO_2 uptakes that exceeded the values of the limestone-benchmark by 300–500% after 30 carbonation-calcination cycles (calcination performed in CO_2 at 900 °C).[23,24]

According to sintering theory, a delay (or even prevention) of the coalescence of adjacent grains requires a deceleration of thermally induced diffusion processes (i.e., surface, grain boundary and volume diffusion).[73,74] Therefore, there are at least three factors that influence the ability of a stabilizer to prevent sintering: (i) the morphology of the stabilizer phase, e.g. as a coating on top of grains or as (nano)particles between grains, (ii) the thickness of the coating/the size of the particles of the stabilizer phase and (iii) the diffusivity of Ca in the stabilizer phase and on its surface and grain boundaries.

The physical separation of two adjacent CaO (or $CaCO_3$) grains increases the length of the diffusional paths, hence increasing the timescale of sintering. Zhang et al.[80] investigated the sintering of two separated spherical sorbent nanoparticles (CaO-CaO or CaO-MgO) during CO_2 sorption conditions and in an inert atmosphere via molecular dynamics simulations. The authors show that the carbonation of previously separated CaO nanoparticles leads to the formation of a handle-like, strongly sintered particle as shown in Figure 7 a, b, indicating that the volume expansion during carbonation is the main contributor to sintering of CaO-based sorbents. Simulations with varying radial distances between the CaO nanoparticles revealed that an increase in the radial distance significantly reduced sintering and in turn increased the CO_2 uptake during carbonation. Indeed, simulations of a stabilized nanoparticle system (CaO-MgO) showed that the presence of a metal oxide stabilizer significantly reduced the degree of inter-particle sintering,

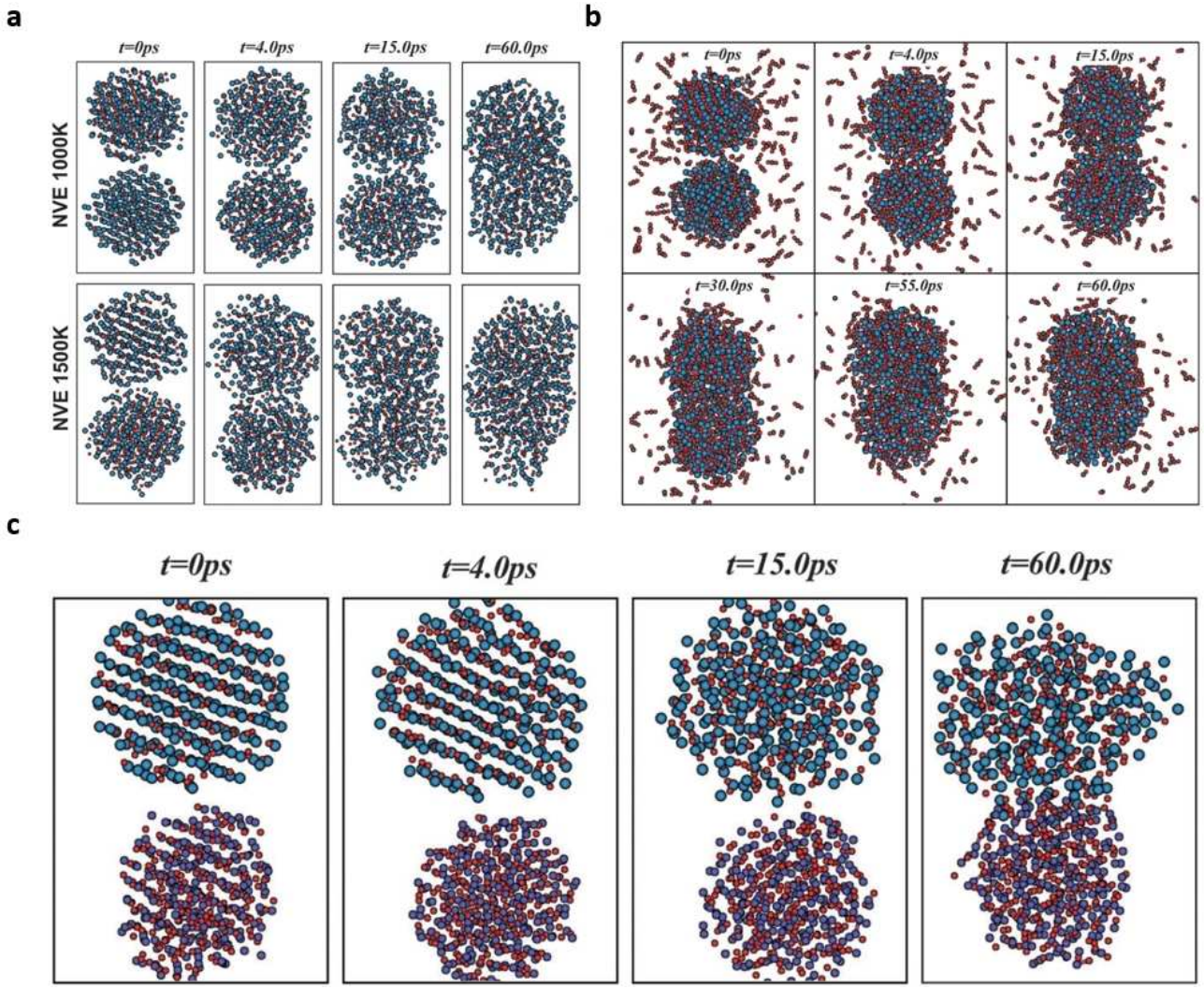

Figure 7. Snapshots of molecular dynamics simulations of (a) sintering of CaO nanoparticles at different temperatures (b) sintering of CaO nanoparticles in the presence of CO_2 and (c) sintering of a CaO and MgO nanoparticle in the presence of CO_2. Reprinted with permission from Ref. [80]; copyright PCCP Owner Societies, 2012.

resulting in a substantially higher CO_2 uptake of the individual CaO nanoparticles, see Figure 7c.

The critical volume fraction of a stabilizer required to achieve a stabilization effect in a large system with many particles has been estimated by percolation theory, which is a mathematical approach to investigate random packings of materials and their connectivity.[81] For example, Jagota et al.[82] investigated a general system of three-dimensional packings of soft and hard spheres via percolation theory to study the influence of the latter on the sintering process. It was shown that the volume fraction of the second, i.e. the stabilizing, phase is a key parameter to control the effective sintering rate. Yet, it is unclear what the most effective distribution of a stabilizer would be, owing to a lack of in-situ observations of both the morphology and stability of the stabilizer and CaO/$CaCO_3$ phases during cyclic operation.

In solids, the speed of volume diffusion becomes significant at elevated temperatures.[83] Most studies argue that the Tammann temperature of the stabilizing phase, which is an indicator for the temperature at which volume diffusion becomes relevant, is a good measure for the stabilizer's ability to prevent CaO and $CaCO_3$ grains from sintering.[12,24,54,72,84] At least two cases must be distinguished here: (i) a stabilizing phase that contains Ca ions and (ii) a stabilizing phase that does not contain Ca ions. For case (i), the diffusion of Ca in the stabilizing phase and on its surface may be directly related to the Tammann temperature of the phase. For case (ii), the Tammann temperature is an indicator for the diffusion of stabilizer ions within the stabilizing phase, and hence can only be an indirect and qualitative measure to evaluate the diffusion of Ca ions. However, the performance of a stabilized CaO-based sorbent is also affected by the sorbent morphology, phase distribution and other factors, as discussed above.[12,73] Therefore, the Tammann temperature can at best be one, but not necessarily the most important, indicator for the performance of the complex stabilizer-CaO system.

Generally, metal oxide stabilizers can be classified into reactive metal oxides and inert metal oxides,[12] whereby the latter do not form mixed oxides with CaO (such as MgO) under CL conditions. The formation of mixed oxides has been reported for a variety of stabilizers including Al_2O_3, ZrO_2 and SiO_2,[17,57,59,64,65,71] see Table 1, and has in some cases been linked to the deactivation of the sorbent. In general, the incorporation of calcium into a CO_2-inert mixed phase leads to a loss in CO_2-reactive CaO, which decreases the maximum CO_2 uptake of the sorbent.[9] Since in many cases metal oxide stabilizers have been added in comparatively high quantities (5–20 wt%), the formation of CO_2-capture-inactive mixed oxides can reduce significantly the maximal theoretical CO_2 uptake of the material. For example, Al_2O_3-stabilized CaO can form at least two Ca-Al mixed oxides under reactive conditions, viz. tricalcium aluminate ($Ca_3Al_2O_6$) and mayenite ($Ca_{12}Al_{14}O_{33}$).[17,23] For ZrO_2- and SiO_2-stabilized CaO, the formation of $CaZrO_3$ and $CaSiO_3$ as well as Ca_2SiO_4 has been observed, respectively.[57,64,66,71] These high-Tammann temperature [$T_T(CaZrO_3) = 1280\,°C$; $T_T(CaSiO_3) = 770\,°C$; $T_T(Ca_2SiO_4) = 1070\,°C$] mixed phases typically form during the heat treatment (i.e. initial calcination) of the sorbent. Hence, for reactive stabilizers, the stabilization effect is linked to the presence of the mixed phase (e.g., $Ca_3Al_2O_6$) rather than the initially added simple oxide (e.g., Al_2O_3). Therefore, an important aspect when choosing a stabilizer is a careful consideration of the phase diagram and the chemical and structural stability of the metal oxide under the temperature swing between CO_2 capture and calcination conditions.

Table 1. Typical metal oxide stabilizers.

Metal oxide	Techniques	Mixed phases reported	Mixed phases favorable[a]	Ref.
Al_2O_3	(in-situ) XRD ^{27}Al-NMR DNP-SENS ^{27}Al-NMR	$Ca_3Al_2O_6$ $Ca_{12}Al_{14}O_{33}$	$Ca_3Al_2O_6$	[23,58,75]
MgO	XRD	–	–	[63,76,77]
MnO_2	XRD	Ca_2MnO_4	Ca_2MnO_4	[78]
Nd_2O_3	–	–	–	[78]
SiO_2	XRD	$CaSiO_3$ α- Ca_2SiO_4 γ-Ca_2SiO_4	α-Ca_2SiO_4 (carb.) γ-Ca_2SiO_4 (calc.)	[65,79]
TiO_2	XRD	$CaTiO_3$	$CaTiO_3$	[78]
Y_2O_3	–	–	–	[78]
ZrO_2	XRD XPS	$CaZrO_3$	$CaZrO_3$	[70–72]

[a] Thermodynamically favorable mixed phase at CaL conditions (600–900 °C, 10 wt% stabilizer).

The phase composition of sorbents stabilized by reactive metal oxides can change with cycle number if (i) several mixed Ca-stabilizer phases exist, (ii) the transformation to the thermodynamically most favorable phase is slow compared to the process timescale (minutes) and (iii) the phase stability is affected by the temperature and atmosphere changes during calcination and carbonation.[9,52] The formation of mixed phases between CaO and a reactive stabilizer has been studied extensively using ex-situ XRD by taking samples after the respective heat and gas treatment steps.[9,12,52] Yet, the dynamics (and intermediate phases) of the respective transformations can only be understood in full detail when utilizing in-situ XRD combined with further structure sensitive techniques.[12,23] For example, Kim et al.[23] studied the phase transformations of $Ca_3Al_2O_6$-stabilized CaO during cyclic operation using a combination of in-situ XRD, ^{27}Al-NMR and EDX-TEM, see Figure 8 and 9. While the as-prepared (calcined) sorbent was composed of CaO, $Ca_3Al_2O_6$ and $Ca_{12}Al_{14}O_{33}$ phases (Figure 8 c–e), in-situ XRD during cyclic operation revealed a complex phase evolution. In the first 10 cycles the fraction of $Ca_3Al_2O_6$ continuously decreased, ultimately disappearing, while the content of the $Ca_{12}Al_{14}O_{33}$ phase increased together with a slight increase in CaO. Between cycles 20 and 30, the phases evolved further, showing a decrease in the fraction of $Ca_{12}Al_{14}O_{33}$ and an increase in CaO, suggesting a segregation of an Al_2O_3 phase. However, since no Al_2O_3 phases could be detected by XRD, an element specific technique, i.e. ^{27}Al-NMR, was applied. Between cycle number 10 and 30, conventional[27] Al-NMR shows Al^{IV} coordination, in agreement with the expected Al coordination in $Ca_3Al_2O_6$ and $Ca_{12}Al_{14}O_{33}$. On the other hand, after 30 cycles dynamic nuclear polarization surface-enhanced (DNP-SENS) ^{27}Al-NMR revealed signatures due to an Al^{VI} coordination owing

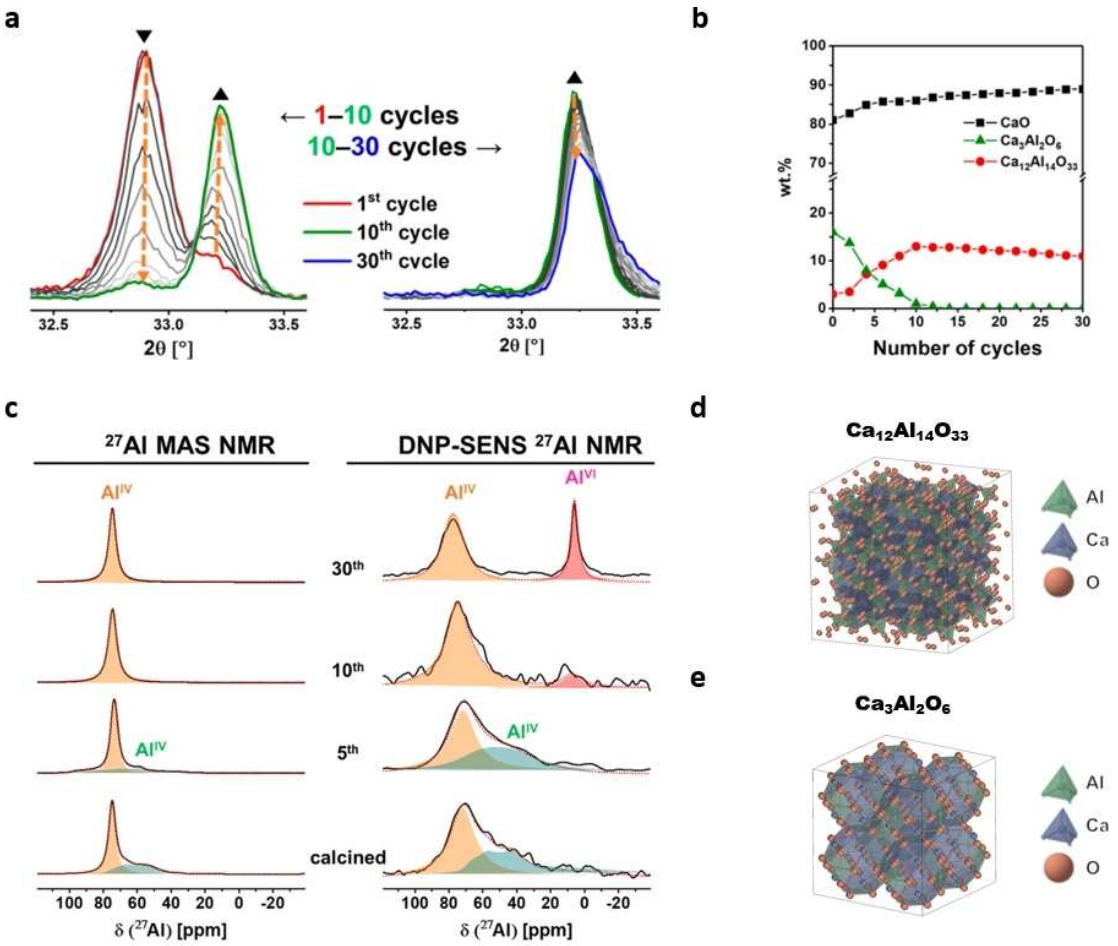

Figure 8. (a) In-situ XRD during cycling of Al_2O_3-stabilized CaO, (b) Rietveld refinement of the in-situ XRD data of (a) and (c) ^{27}Al-MAS-NMR and DNP-SENS NMR of Al_2O_3-stabilized CaO over cycling. Adapted with permission from Ref. [23]; copyright American Chemical Society, 2018. (d) Crystalline structure of mayenite ($Ca_{12}Al_{14}O_{33}$) and (e) crystalline structure of calcium aluminate ($Ca_3Al_2O_6$).

to α-Al_2O_3 (Figure 8c). However, according to the CaO-Al_2O_3 equilibrium phase diagram,[85] between 650–900 °C and with a Al:Ca ratio of 1:9, CaO and $Ca_3Al_2O_6$ are the thermodynamically stable phases while Al_2O_3 is not expected to be present under these conditions.

At the surface of the CaO particles, the nanoparticles of the stabilizing phase tend to agglomerate, reducing their effectiveness to act as a physical barrier against sintering, leading in turn to a reduced CO_2 uptake of the material. For example in the study of Kim et al., alumina-rich phases are well distributed after the initial calcination step but segregate towards the particle surface to form large agglomerates over cycling, which is confirmed via EDX-TEM, see Figure 9a. TEM analysis clearly shows the segregation of an Al-rich phase in the form of nanoparticles of 200 nm in size and their migration to the surface. Interestingly, this surface-enrichment of Al_2O_3 through phase-segregation from the Ca-Al mixed oxides was identified to trigger the deactivation of the sorbents (and material sintering). Yet, the nature of this phase transformation remains unclear.

Indeed, for a variety of stabilizers the segregation of (nano) particles of the stabilizing phase from bulk CaO to the surface (with or without phase change) has been observed during heat treatment and over cycling.[23,57,65] Yoon et al. investigated $CaZrO_3$- and ZrO_2-stabilized CaO, synthesized via a sol-gel method and observed the segregation of Ca-Zr mixed phases to the particle surface after cyclic operation. After cycling, segregated Zr-rich particles with a diameter of several hundred nm were observed via back-scattered electron microscopy. However, the authors did not identify the surface segregated phases via surface-sensitive techniques. Koirala et al.[69] investigated $CaZrO_3$-stabilized CaO, see Figure 10 a, b, with XPS to identify changes in the phase composition near the particle surface. Based on the Ca2p XPS spectrum shown in Figure 10c–f, the authors concluded that the quantity of $CaZrO_3$ nanoparticles on the surface of CaO particles increased after heat treatment with the amount of zirconia added until a saturated value was achieved. The best performing sorbent had a bulk ratio of Ca/Zr = 5.[69] High-resolution TEM studies revealed that sorbents containing Zr/Ca ratios of 4:10 and 5:10 show an increase in sorbent particle size from 4–6 nm and 4–5 nm,

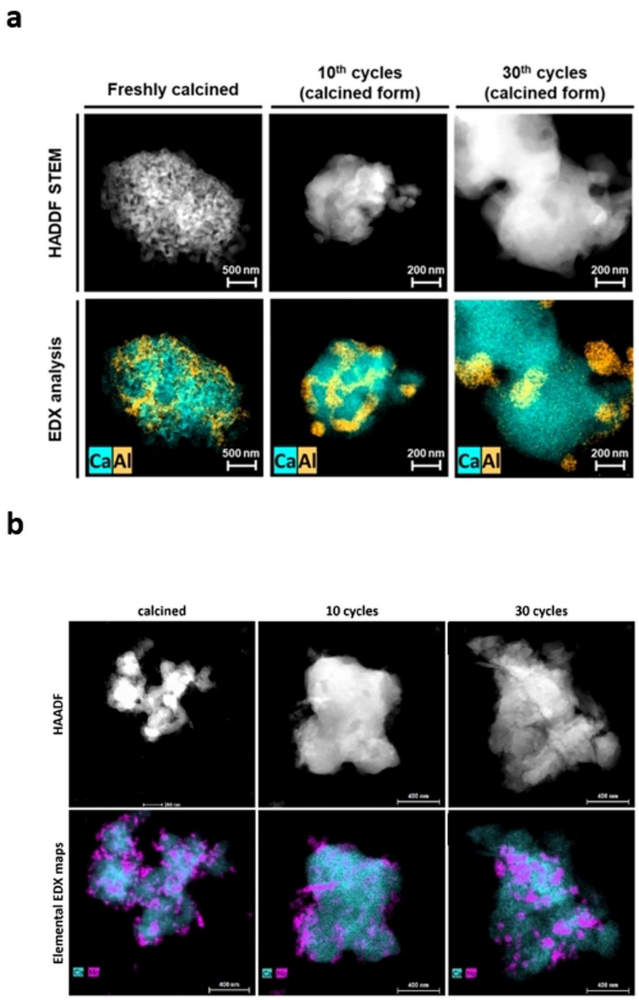

Figure 9. (a) HAADF micrographs and TEM-EDX mapping of Ca and Al of $Ca_3Al_2O_6$-stabilized CaO. Reprinted with permission from [23]; copyright American Chemical Society, 2018. (b) HAADF micrographs and TEM-EDX mapping of Ca and Mg of MgO-stabilized CaO. Reprinted with permission from Ref. [76]; copyright Wiley-VCH, 2016.

respectively, to 24–58 nm and 12–32 nm after 250 isothermal cycles (i.e., calcination in N_2 and carbonation in 15 vol% CO_2 at 700 °C).[69] Hence, the growth of particle size was correlated with the amount of stabilizer added, with increasing amounts of stabilizer leading to smaller sorbent particle sizes after cycling.

Turning to SiO_2-stabilized CaO-based sorbents, several mixed oxide phases and polymorphs exist in the Ca-Si-O system, depending on the Ca/Si ratio and the respective pre-treatment and operating temperatures. Wang et al.[79] showed that the calcination temperature and time influence the formation of mixed Ca-Si oxides for a given sorbent composition, i.e. the solid-state reaction to the thermodynamically favorable mixed oxide is slow. For example, after calcination at 900 °C for 1 h four Si-containing phases were detected: Ca_2SiO_4, $CaSiO_3$ (calcium silicate and wollastonite polymorphs) and SiO_2. However, based on the CaO-SiO_2 phase diagram, only Ca_2SiO_4 should be observed (8 wt% SiO_2, i.e. Ca/Si = 12, 900 °C), indicating that the transformation to the thermodynamically favorable phase was not completed. In addition, both α- and γ-phases of Ca_2SiO_4 exist, and the transition between these two polymorphs is observed at around 700 °C. Therefore, the stabilizing phase in SiO_2-CaO sorbents may transform between different phases owing to the temperature swing between calcination (typically around 900 °C) and carbonation (typically around 650 °C) as well as the incomplete transformation to the thermodynamically most favorable phase during the first heat treatment. Yet, the influence of these phase transformations during cycling has not been investigated in detail.

Inert metal oxide stabilizers such as MgO do not form mixed phases with CaO and do not form carbonates at typical CaL conditions (i.e., $T > 600$ °C).[54,63,76] However, a similar tendency for agglomeration of the stabilizer phases as observed in reactive stabilizers (e.g., Al_2O_3 or ZrO_2), is observed for inert stabilizers.[12,23,76] In an early study, Liu et al.[51] used a wet-mixing method to synthesize MgO-stabilized CaO with an almost constant CO_2 uptake of 0.59 $g_{CO_2}/g_{Sorbent}$ over the course of 24 cycles (25 wt% MgO, carbonation at 650 °C and calcination at 900 °C in N_2). The authors showed via EDX-TEM that MgO forms agglomerates on the surface of CaO particles. It was argued that these agglomerates act as barriers against sintering of CaO. In a more recent study, Kurlov et al.[76] investigated the distribution of MgO and changes thereof over cycling in MgO-stabilized CaO-based sorbents using EDX-TEM, see Figure 9b. Initially, nanoparticles of MgO of diameters up to 50 nm, were evenly distributed on the surface of CaO grains in the as-prepared sorbent. After 30 cycles, the MgO nanoparticles agglomerated leading to an increase in particle size (100–200 nm). It was argued that larger MgO nanoparticles were less effective in mitigating sintering and hence led to a decrease in the CO_2 uptake. Naeem et al., who synthesized hollow microspheres of CaO stabilized by MgO,[24] also observed an increase in the size of the MgO nanoparticles over cycling. The shell of these microspheres consists of CaO and MgO nanoparticles. Over cycling, the size of the MgO nanoparticles increased from 15–35 nm in the as-prepared sorbents to about 80–100 nm after 10 cycles under realistic conditions (i.e., calcination under CO_2 at 900 °C). However, the authors observed a homogeneous distribution of the MgO nanoparticles in the sorbent even after cycling and no significant segregation of larger MgO aggregates from CaO.

3.3. Alkali metal salt-modified CaO-based sorbents

An actively debated question is whether the addition of alkali metal salts such as Na_2CO_3,[11,22,86] K_2CO_3,[11,86,87] Li_2CO_3,[87] NaCl[86,87] or KCl[86,87] can improve the cyclic CO_2 uptake of CaO-based CO_2 sorbents. Most alkali metal salts (here only considering chlorides and carbonates) melt at similar temperatures as $CaCO_3$ [T_M(ACl, A_2CO_3) = 600–900 °C with A = Li, Na, K, Rb, Cs; $T_M(CaCO_3)$ = 825 °C] and have significantly lower Tammann-temperatures than CaO [T_T(ACl, A_2CO_3) = 300-450 °C; T_T(CaO) = 1313 °C].[9,12,70,86] Hence, most studies argue that alkali metal salts may act as promoters of the CO_2 uptake (e.g., via kinetic effects)

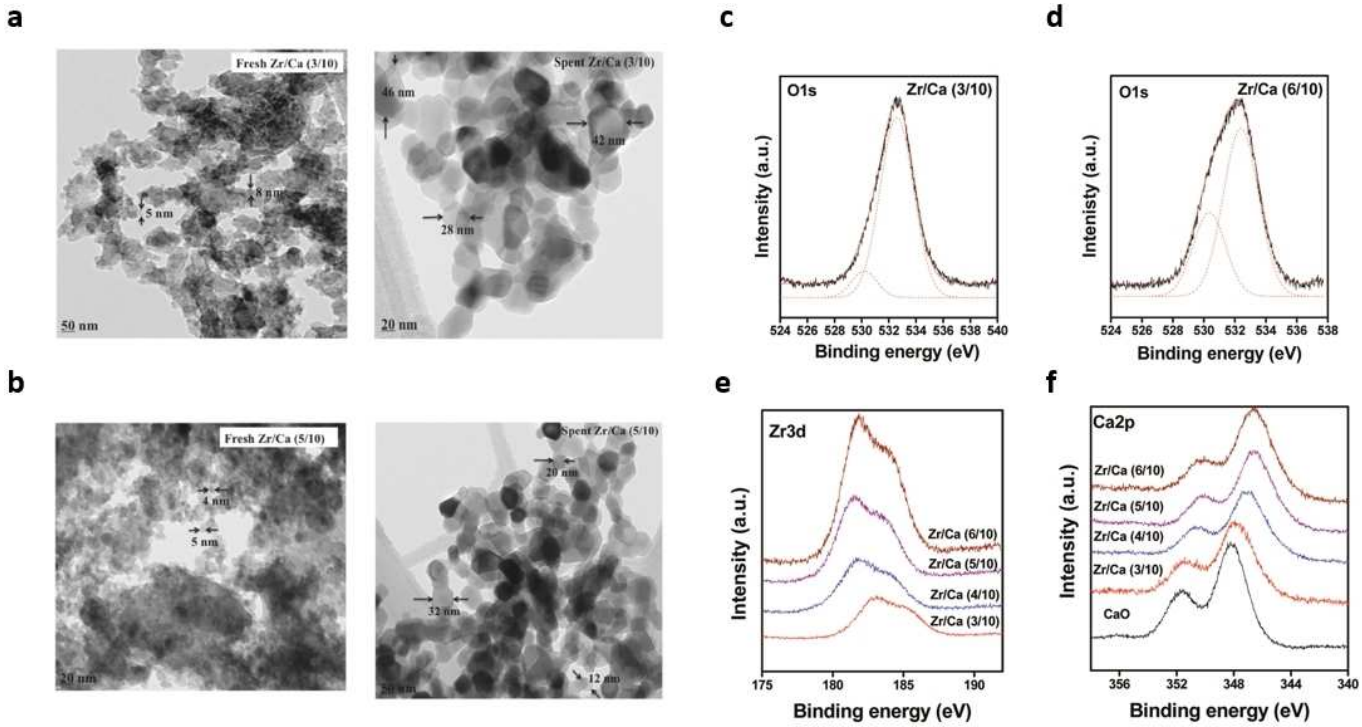

Figure 10. (a) High-resolution TEM images of flame-spray-synthesized $CaZrO_3$-stabilized CaO nanoparticles before and after cycling (calcined). (b) O1s XPS spectra of $CaZrO_3$-stabilized CaO (c-f) Ca2p and Zr3d XPS spectra of sorbents with various Zr contents. Adapted with permission from Ref. [69]; copyright American Chemical Society, 2011.

in contrast to metal oxides, which act as stabilizers against sintering.

The cyclic CO_2 uptake performance of alkali metal-modified CaO varies strongly depending on the nature of the alkali metal (i.e., Li, Na, K, Rb and Cs), the precursors used for synthesis (e.g., Na_2CO_3 vs. NaCl) and the content of alkali metal salt added.[11,70,88] However, a general trend of a decreased CO_2 uptake with increasing alkali metal content seems to hold for most studies. For high contents of Na and K (i.e., several mol%), independent of the precursor used, various authors have shown that the CO_2 uptake performance is decreased, possibly due to enhanced sintering effects.[22,86] In such cases, the addition of alkali metals leads to an inferior performance over cycling showing CO_2 uptakes as low as 0.05 $g_{CO_2}/g_{Sorbent}$ (e.g., 20 wt% NaOH, wet-impregnated)[87] already during the first carbonation step (40% CO_2, 600 °C, 5 h).

For low alkali metal contents, some studies have observed a strong promotional effect of alkali metal salts such as NaCl[86] (2 wt%, wet impregnation, uptake 10th cycle 0.48 $g_{CO_2}/g_{Sorbent}$), KCl (2 wt%, wet impregnation, uptake 10th cycle 0.50 $g_{CO_2}/g_{Sorbent}$) and NaCl from sea salt (ca. 0.13 wt% NaCl, wet impregnation, uptake 10th cycle 0.33 $g_{CO_2}/g_{Sorbent}$). It has been proposed that there is an appreciable effect of alkali metals on the kinetics of the carbonation and calcination reactions which may enhance the CO_2 uptake performance[9] For example, Wieczorek-Ciurowa et al.[89] have shown that the decomposition temperature of calcite is reduced by about 10 °C by the addition of NaCl, i.e. alkali metals can shift the CaO/$CaCO_3$ equilibrium. A similar shift of the decomposition temperature by about 10 °C has been reported by Xu et al. for the addition of KCl and KOH.[86] Other authors have reported that alkali metals may also positively affect the diffusion process of CO_2 in the product layer of $CaCO_3$. For example, Gonzalez et al.[90] reported that for wet-impregnated limestone (0.05–0.5 M KCl/K_2CO_3 aqueous solution) the conversion rate of CaO in the diffusion-controlled carbonation regime was enhanced by the addition of either KCl or K_2CO_3 compared to the pristine limestone benchmark. The authors concluded that the incorporation of potassium impurities in the sorbent promotes the diffusional processes during carbonation (i.e., the diffusion of CO_2 through the $CaCO_3$ product layer). However, there is limited fundamental understanding of how low alkali metals contents may affect diffusional processes or promote the performance of CaO-based sorbents. Therefore, this area deserves further research using advanced characterization techniques to understand the underlying mechanisms of promotion.

Alkali metals can react with CO_2 to form carbonates of the form A_2CO_3 (A = Na, K, Li, Cs). If present in a CaO environment, some alkali metals may form mixed bicarbonates of the structural formula $A_2Ca(CO_3)_2$ during carbonation. Similar to other alkali metal salts, these mixed bicarbonates have a low melting point (e.g., $T_M[Na_2Ca(CO_3)_2] = 810$ °C). Recently, using in-situ XRD, Lee et al.[22] have shown that the mixed bicarbonate $Na_2Ca(CO_3)_2$ forms in Na_2CO_3-impregnated CaO (see Figure 11a) during carbonation (i.e., 600–700 °C in 15 vol% CO_2). The authors provide a formation mechanism for the mixed bicar-

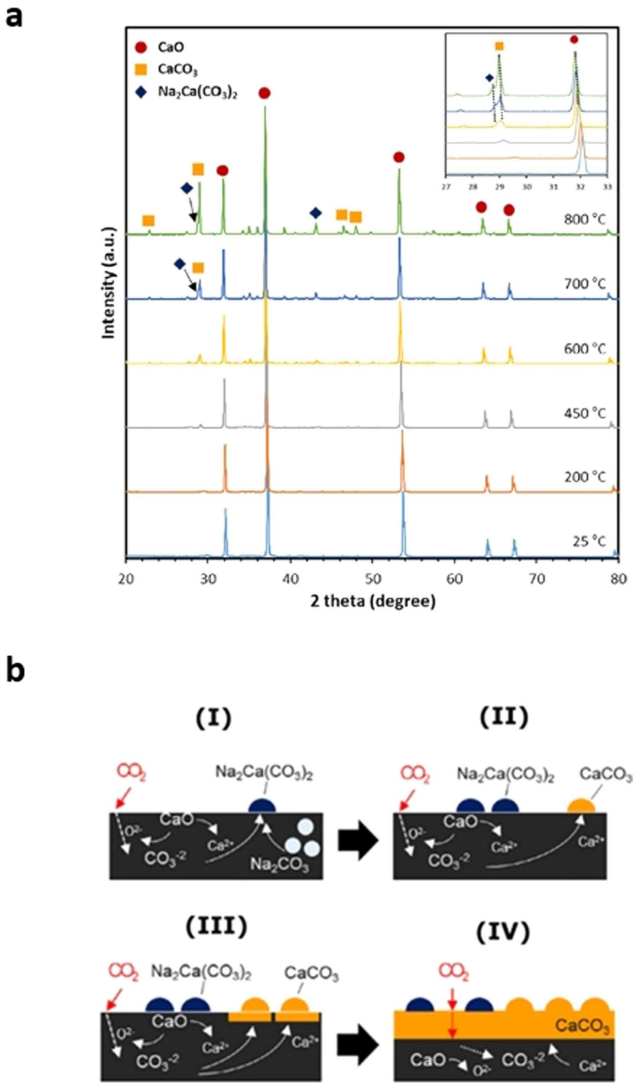

Figure 11. (a) In-situ XRD of Na_2CO_3-wet-impregnated CaO between 25 °C and 800 °C (b) Proposed formation mechanism of $Na_2Ca(CO_3)_2$. Adapted with permission from Ref. [22]; copyright Elsevier, 2018.

bonate and propose that it forms during the initial carbonation step, see Figure 11b. Hence, the study concludes that the mixed bicarbonate may form at the surface of the CaO particles and proposes the formation mechanism shown in Figure 11 b. Currently, we have no in-depth understanding of how these mixed phases may affect the performance of alkali-metal promoted CaO.

In a study aiming to obtain a comprehensive description of the effect of different alkali metal salts on the CO_2 uptake of CaO, Reddy et al. probed the influence of different alkali metals and precursors (ACl, AOH, and A_2CO_3 with A = Li, Na, K, Rb, Cs) via the wet impregnation of CaO using loadings of 10 wt % and 20 wt %.[87] The authors studied the CO_2 uptake in the first carbonation cycle at temperatures between 50 °C and 750 °C, showing that the CO_2 uptake in the first carbonation cycle increases with the electropositivity and ionic radii of the alkali metal (Cs > Rb > K > Na > Li), as shown in Figure 12. The authors hypothesize that alkali metals influence the affinity of CaO towards acidic CO_2, resulting in turn in an improved CO_2 uptake compared to CaO, even at low temperatures (i.e., 50 °C). XPS analysis of Cs_2CO_3-promoted CaO indicates that CO_2 preferentially reacts with CsO_2, which forms during calcination. Yet, we currently lack a mechanistic explanation of how the electropositivity of the ion or the ionic radii may affect the affinity of the sorbent towards CO_2. Indeed, morphological parameters such as the pore size distribution, pore volume and BET surface area have not been investigated in this study except for Cs/CaO and the CaO benchmark. Therefore, the results might as well be related to varying effects of the different alkali metals and precursors on the morphological characteristics of the sorbents rather than a change in their affinity towards CO_2, as has been reported before.[70,91] To conclude, a better understanding of the effect of alkali metals on the textural properties of CaO during cycling will be pivotal to elucidate the effect of alkali metals on the CO_2 uptake of CaO.

4. Summary and Outlook

In the last decade, advanced characterization techniques have been applied increasingly to the field of CaO-based CO_2 sorbents and have provided novel insights into the structural and textural changes that occur during the carbonation and calcination reaction on the nanoscale. For example, AFM suggests an island-type growth mode of $CaCO_3$ on CaO in the early stage of carbonation. Furthermore, a better understanding of the morphological changes that occur at different stages during the carbonation step has been obtained by in-situ XRD, (U)SAXS and X-ray tomography. In the future, a combination of atomic scale simulations and in-situ visualization of the product layer formation should improve our understanding of the kinetics of the carbonation reaction in both the reaction- and the diffusion-controlled regimes. In the case of stabilized and/or promoted CaO, some insights into the sintering mechanism have been obtained, with molecular dynamics simulations indicating that the volume expansion during carbonation is the main cause for sintering and that the effect of a stabilizer is to increase the length of the (diffusional) pathways between the individual CaO ($CaCO_3$) grains. In addition, the application of in-situ XRD, NMR and EDX-TEM characterization has provided insight into the stabilization and deactivation mechanisms of stabilized CaO during repeated cycling. However, studies on alkali metal-modified CaO-based sorbents have largely lacked results from advanced characterization techniques, such that our current fundamental understanding of the promotion and deactivation mechanisms is very limited. In the future, studying the nanoscale interaction of stabilizers and promoters with $CaO/CaCO_3$ will be critical to guide the rational design of the next generation of CaO-based CO_2 sorbents.

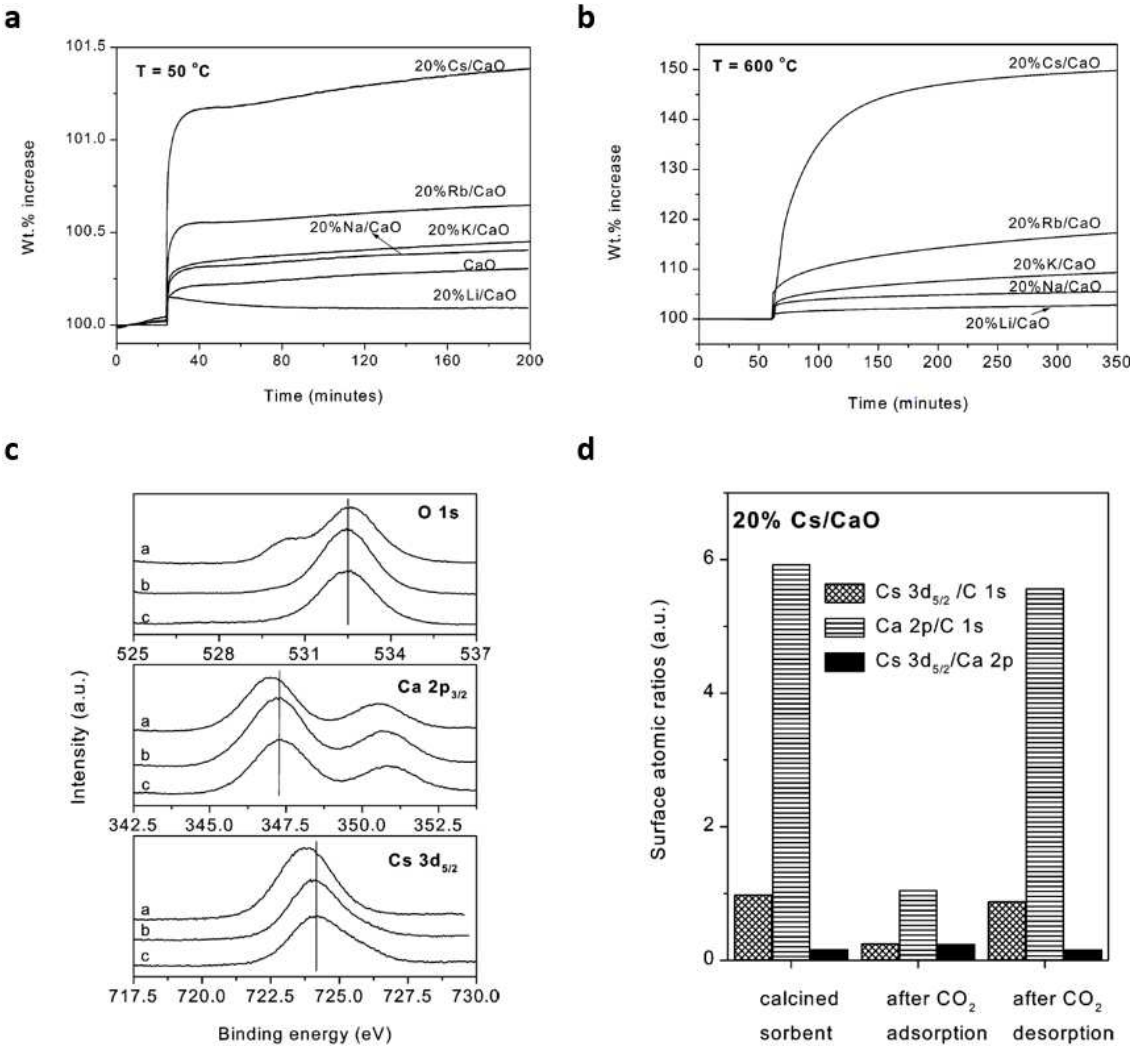

Figure 12. TGA measurements of CO_2 sorption on alkali-metal doped CaO at (a) 50 °C and (b) at 500 °C; (c) XPS spectra of sorbents before and after reaction with CO_2 and d) atomic ratios of Cs to Ca at the surface over the course of one carbonation-calcination cycle for Cs_2CO_3-promoted CaO. Adapted with permission from Ref. [87]; Copyright American Chemical Society, 2004.

Acknowledgements

The authors acknowledge funding from the European Research Council (ERC) under the European Union's Horizon 2020 research and innovation programme under grant agreement No. 819573 and the Swiss National Science Foundation (200020_156015).

Conflict of Interest

The authors declare no conflict of interest.

Keywords: advanced characterization · calcium oxide · CO_2 sorbent · promoters · stabilizers

[1] R. K. Pachauri, L. A. Meyer, Climate Change 2014: Synthesis Report. Contribution of Working Groups I, II and III to the Fifth Assessment Report of the Intergovernmental Panel on Climate Change., **2014**.
[2] M. Collins, R. Knutti, J. Arblaster, J.-L. Dufresne, T. Fichefet, P. Friedlingstein, X. Gao, W. J. Gutowski, T. Johns, G. Krinner, M. Shongwe, C. Tebaldi, A. J. Weaver, M. Wehner, in *Clim. Chang. 2013 - Phys. Sci. Basis* (Ed.: Intergovernmental Panel on Climate Change), Cambridge University Press, Cambridge, **2013**, pp. 1029–1136.
[3] NASA, Local CO_2 Concentration at Mauna Loa Observatory, Hawaii, USA, **2020**.
[4] M. Bui, C. S. Adjiman, A. Bardow, E. J. Anthony, A. Boston, S. Brown, P. S. Fennell, S. Fuss, A. Galindo, L. A. Hackett, J. P. Hallett, H. J. Herzog, G. Jackson, J. Kemper, S. Krevor, G. C. Maitland, M. Matuszewski, I. S. Metcalfe, C. Petit, G. Puxty, J. Reimer, D. M. Reiner, E. S. Rubin, S. A. Scott, N. Shah, B. Smit, J. P. M. Trusler, P. Webley, J. Wilcox, N. Mac Dowell, *Energy Environ. Sci.* **2018**, *11*, 1062–1176.
[5] D. T. Whipple, P. J. A. Kenis, *J. Phys. Chem. Lett.* **2010**, *1*, 3451–3458.
[6] P. Anbu, C. H. Kang, Y. J. Shin, J. S. So, *Springerplus* **2016**, *5*, 250.
[7] J. Artz, T. E. Müller, K. Thenert, J. Kleinekorte, R. Meys, A. Sternberg, A. Bardow, W. Leitner, *Chem. Rev.* **2018**, *118*, 434–504.
[8] E. Alper, O. Yuksel Orhan, *Petroleum* **2017**, *3*, 109–126.
[9] S. A. Salaudeen, B. Acharya, A. Dutta, *J. CO2 Util.* **2018**, *23*, 179–199.
[10] T. H. Wang, D. C. Xiao, C. H. Huang, Y. K. Hsieh, C. S. Tan, C. F. Wang, *J. Hazard. Mater.* **2014**, *270*, 92–101.

[11] A. Al-Mamoori, H. Thakkar, X. Li, A. A. Rownaghi, F. Rezaei, *Ind. Eng. Chem. Res.* **2017**, *56*, 8292–8300.
[12] A. M. Kierzkowska, R. Pacciani, C. R. Müller, *ChemSusChem* **2013**, *6*, 1130–1148.
[13] A. MacKenzie, D. L. Granatstein, E. J. Anthony, J. C. Abanades, *Energy Fuels* **2007**, *21*, 920–926.
[14] G. S. Grasa, J. C. Abanades, *Ind. Eng. Chem. Res.* **2006**, *45*, 8846–8851.
[15] A. Silaban, M. Narcida, D. P. Harrison, *Resour. Conserv. Recycl.* **1992**, *7*, 139–153.
[16] S. M. Kim, P. M. Abdala, M. Broda, D. Hosseini, C. Copéret, C. Müller, *ACS Catal.* **2018**, *8*, 2815–2823.
[17] M. A. Naeem, A. Armutlulu, A. Kierzkowska, C. R. Müller, *Energy Procedia* **2017**, *114*, 158–166.
[18] M. A. Naeem, A. Armutlulu, M. Broda, D. Lebedev, C. R. Müller, *Faraday Discuss.* **2016**, *192*, 85–95.
[19] J. M. Valverde, P. E. Sanchez-Jimenez, L. A. Perez-Maqueda, *Appl. Energy* **2015**, *138*, 202–215.
[20] A. Armutlulu, M. A. Naeem, H. J. Liu, S. M. Kim, A. Kierzkowska, A. Fedorov, C. R. Müller, *Adv. Mater.* **2017**, *29*, 1702896.
[21] C. Luo, Q. Shen, N. Ding, Z. Feng, Y. Zheng, C. Zheng, *Chem. Eng. Technol.* **2012**, *35*, 547–554.
[22] C. H. Lee, S. W. Choi, H. J. Yoon, H. J. Kwon, H. C. Lee, S. G. Jeon, K. B. Lee, *Chem. Eng. J.* **2018**, *352*, 103–109.
[23] S. M. Kim, W. C. Liao, A. M. Kierzkowska, T. Margossian, D. Hosseini, S. Yoon, M. Broda, C. Copéret, C. R. Müller, *Chem. Mater.* **2018**, *30*, 1344–1352.
[24] M. A. Naeem, A. Armutlulu, Q. Imtiaz, F. Donat, R. Schäublin, A. Kierzkowska, C. R. Müller, *Nat. Commun.* **2018**, *9*, 2408.
[25] S. M. Kim, A. M. Kierzkowska, M. Broda, C. R. Müller, *Energy Procedia* **2017**, *114*, 220–229.
[26] S. M. Kim, A. Armutlulu, A. M. Kierzkowska, C. R. Müller, *ACS Appl. Mater. Interfaces* **2019**, *2*, 6461–6471.
[27] D. P. Hanak, E. J. Anthony, V. Manovic, *Energy Environ. Sci.* **2015**, *8*, 2199–2249.
[28] A. J. Dedman, A. J. Owen, *Trans. Faraday Soc.* **1962**, *58*, 2027–2035.
[29] R. Barker, *J. Appl. Chem. Biotechnol.* **1973**, *23*, 733–742.
[30] D. Alvarez, J. Carlos Abanades, *Ind. Eng. Chem. Res.* **2005**, *44*, 5608–5615.
[31] D. Mess, A. F. Sarofim, J. P. Longwell, *Energy Fuels* **1999**, *13*, 999–1005.
[32] J. S. Dennis, R. Pacciani, *Chem. Eng. Sci.* **2009**, *64*, 2147–2157.
[33] R. Pacciani, C. R. Müller, J. F. Davidson, J. S. Dennis, A. N. Hayhurst, *Can. J. Chem. Eng.* **2008**, *86*, 356–366.
[34] Z.-S. Li, F. Fang, X.-Y. Tang, N.-S. Cai, *Energy and Fuels* **2012**, *26*, 2473–2482.
[35] A. Benedetti, J. Ilavsky, C. Segre, M. Strumendo, *Chem. Eng. J.* **2019**, *355*, 760–776.
[36] M. T. Dunstan, S. A. Maugeri, W. Liu, M. G. Tucker, O. O. Taiwo, B. Gonzalez, P. K. Allan, M. W. Gaultois, P. R. Shearing, D. A. Keen, A. E. Phillips, M. T. Dove, S. A. Scott, J. S. Dennis, C. P. Grey, *Faraday Discuss.* **2016**, *192*, 217–240.
[37] A. Biasin, C. U. Segre, M. Strumendo, *Cryst. Growth Des.* **2015**, *15*, 5188–5201.
[38] A. Biasin, C. U. Segre, G. Salviulo, F. Zorzi, M. Strumendo, *Chem. Eng. Sci.* **2015**, *127*, 13–24.
[39] J. Chen, L. Duan, Z. Sun, *Environ. Sci. Technol.* **2019**, *53*, 2249–2259.
[40] J. M. Valverde, P. E. Sanchez-Jimenez, L. A. Perez-Maqueda, *J. Phys. Chem. C* **2015**, *119*, 1623–1641.
[41] J. M. Valverde, S. Medina, *Phys. Chem. Chem. Phys.* **2015**, *17*, 21912–21926.
[42] C. Rodriguez-Navarro, E. Ruiz-Agudo, A. Luque, A. B. Rodriguez-Navarro, M. Ortega-Huertas, *Am. Mineral.* **2009**, *94*, 578–593.
[43] R. Besson, L. Favergeon, *J. Phys. Chem. C* **2013**, *117*, 8813–8821.
[44] H. Sun, J. Wang, X. Liu, B. Shen, C. M. A. Parlett, G. O. Adwek, E. John Anthony, P. T. Williams, C. Wu, *J. Mater. Chem. A* **2019**, *7*, 9977–9987.
[45] S. K. Bhatia, D. D. Perlmutter, *AIChE J.* **1981**, *27*, 247–254.
[46] S. K. Bhatia, D. D. Perlmutter, *AIChE J.* **1983**, *29*, 79–86.
[47] P. Sun, J. R. Grace, C. J. Lim, E. J. Anthony, *Chem. Eng. Sci.* **2008**, *63*, 47–56.
[48] R. Besson, D. Tingaud, L. Favergeon, *J. Phys. Chem. C* **2019**, *123*, 21825–21837.
[49] Z. Sun, S. Luo, P. Qi, L. S. Fan, *Chem. Eng. Sci.* **2012**, *81*, 164–168.
[50] F. Donat, C. R. Müller, *Chem. Eng. J.* **2018**, *336*, 544–549.
[51] W. G. Liu, N. W. L. Low, B. Feng, G. Wang, J. C. Diniz Da Costa, *Environ. Sci. Technol.* **2010**, *44*, 841–847.
[52] W. Liu, H. An, C. Qin, J. Yin, G. Wang, B. Feng, M. Xu, *Energy Fuels* **2012**, *26*, 2751–2767.
[53] A. Akgsornpeak, T. Witoon, T. Mungcharoen, J. Limtrakul, *Chem. Eng. J.* **2014**, *237*, 189–198.
[54] K. Wang, P. T. Clough, P. Zhao, E. J. Anthony, *J. Mater. Chem. A* **2019**, *7*, 9173–9182.
[55] M. A. Naeem, A. Armutlulu, Q. Imtiaz, C. R. Müller, *ChemPhysChem* **2017**, *18*, 3280–3285.
[56] A. Kurlov, A. Armutlulu, F. Donat, A. R. Studart, C. R. Müller, *Ind. Eng. Chem. Res.* **2020**, *59*, 7182–7188.
[57] H. J. Yoon, K. B. Lee, *Chem. Eng. J.* **2019**, *355*, 850–857.
[58] B. Azimi, M. Tahmasebpoor, P. E. Sanchez-Jimenez, A. Perejon, J. M. Valverde, *Chem. Eng. J.* **2019**, *358*, 679–690.
[59] C. Chi, Y. Li, W. Zhang, Z. Wang, *Appl. Energy* **2019**, *251*, 113382.
[60] S. F. Wu, Q. H. Li, J. N. Kim, K. B. Yi, *Ind. Eng. Chem. Res.* **2008**, *47*, 180–184.
[61] N. J. Amos, M. Widyawati, S. Kureti, D. Trimis, A. I. Minett, A. T. Harris, T. L. Church, *J. Mater. Chem. A* **2014**, *2*, 4332.
[62] J. Park, K. B. Yi, *Int. J. Hydrogen Energy* **2012**, *37*, 95–102.
[63] X. Yang, L. Zhao, S. Yang, Y. Xiao, *Asia-Pac. Chem.* **2013**, *8*, 906–915.
[64] M. Wang, C. G. Lee, C. K. Ryu, *Int. J. Hydrogen Energy* **2008**, *33*, 6368–6372.
[65] M. Benitez-Guerrero, J. M. Valverde, A. Perejon, P. E. Sanchez-Jimenez, L. A. Perez-Maqueda, *Appl. Energy* **2018**, *210*, 108–116.
[66] P. E. Sanchez-Jimenez, L. A. Perez-Maqueda, J. M. Valverde, *Appl. Energy* **2014**, *118*, 92–99.
[67] J. M. Valverde, A. Perejon, L. A. Perez-Maqueda, *Environ. Sci. Technol.* **2012**, *46*, 6401–6408.
[68] W. Peng, Z. Xu, C. Luo, H. Zhao, *Environ. Sci. Technol.* **2015**, *49*, 8237–8245.
[69] R. Koirala, K. R. Gunugunuri, S. E. Pratsinis, P. G. Smirniotis, *J. Phys. Chem. C* **2011**, *115*, 24804–24812.
[70] Y. Xu, C. Luo, Y. Zheng, H. Ding, Q. Wang, Q. Shen, X. Li, L. Zhang, *RSC Adv.* **2016**, *6*, 79285–79296.
[71] K. S. Sultana, D. T. Tran, J. C. Walmsley, M. Rønning, D. Chen, *Ind. Eng. Chem. Res.* **2015**, *54*, 8929–8939.
[72] M. Broda, C. R. Müller, *Fuel* **2014**, *127*, 94–100.
[73] P. M. Derlet, E. A. Olevsky, *Solutions* **2011**.
[74] E. A. Olevsky, Present. Tech. Univ. Darmstadt **2011**.
[75] J. Jing, T. Li, X. Zhang, S. Wang, J. Feng, W. A. Turmel, W. Li, *Appl. Energy* **2017**, *199*, 225–233.
[76] A. Kurlov, M. Broda, D. Hosseini, S. J. Mitchell, J. Pérez-Ramírez, C. R. Müller, *ChemSusChem* **2016**, *9*, 2380–2390.
[77] M. Broda, A. M. Kierzkowska, C. R. Müller, *Adv. Funct. Mater.* **2014**, *24*, 5753–5761.
[78] Y. Hu, W. Liu, H. Chen, Z. Zhou, W. Wang, J. Sun, X. Yang, X. Li, M. Xu, *Fuel* **2016**, *181*, 199–206.
[79] H. Wang, Q. Zhang, H. Yang, H. Sun, *Ceram. Int.* **2008**, *34*, 1405–1408.
[80] L. Zhang, Y. Lu, M. Rostam-Abadi, *Phys. Chem. Chem. Phys.* **2012**, *14*, 16633–16643.
[81] A. A. Saberi, *Phys. Rep.* **2015**, *578*, 1–32.
[82] A. Jagota, G. W. Scherer, *J. Am. Ceram. Soc.* **1995**, *78*, 521–528.
[83] A. Khawam, D. R. Flanagan, *J. Phys. Chem. B* **2006**, *110*, 17315–17328.
[84] M. A. Naeem, A. Armutlulu, Q. Imtiaz, C. R. Müller, *ChemPhysChem* **2017**, *18*, 3280–3285.
[85] R. Salomão, V. L. Ferreira, I. R. de Oliveira, A. D. V. Souza, W. R. Correr, *J. Eur. Ceram. Soc.* **2016**, *36*, 4225–4235.
[86] Y. Xu, H. Ding, C. Luo, Y. Zheng, Q. Zhang, X. Li, J. Sun, L. Zhang, *ACS Sustainable Chem. Eng.* **2018**, *6*, 11677–11684.
[87] E. P. Reddy, P. G. Smirniotis, *J. Phys. Chem. B* **2004**, *108*, 7794–7800.
[88] L. Huang, C. Xu, R. Ren, Q. Zheng, Z. Wang, B. Louis, Q. Wang, *Sustainable Energy Fuels* **2018**, *2*, 68–72.
[89] K. Wieczorek-ciurowa, J. Paulik, F. Paulik, *Thermochim. Acta* **1980**, *38*, 157–164.
[90] B. González, J. Blamey, M. McBride-Wright, N. Carter, D. Dugwell, P. Fennell, J. C. Abanades, *Energy Procedia* **2011**, *4*, 402–409.
[91] Y. Xu, H. Ding, C. Luo, Q. Zhang, Y. Zheng, X. Li, Y. Hu, L. Zhang, *Energy and Fuels* **2018**, *32*, 8571–8578.

Manuscript received: August 31, 2020
Revised manuscript received: October 11, 2020
Accepted manuscript online: October 13, 2020
Version of record online: October 27, 2020